Progress In Electromagnetics Research Letters, Vol. 23, 29–38, 2011

NONLINEAR TRAVELING-WAVE FIELD-EFFECT TRANSISTORS FOR MANAGING DISPERSION-FREE ENVELOPE PULSES

K. Narahara

Graduate School of Science and Engineering
Yamagata University
4-3-16 Jonan, Yonezawa, Yamagata 992-8510, Japan

Abstract—A specialized type of traveling-wave field-effect transistor (TWFET), the gate and drain lines of which contain series capacitors, series inductors, shunt capacitors, and shunt inductors, is considered to provide a platform to manage unattenuated dispersion-free envelope pulses. Because of the nonlinearity caused by the gate-source Schottky capacitance, the dispersive distortion is well compensated. Moreover, the FET gain can cancel the wave attenuation caused by electrode losses. This paper discusses the design criteria of a TWFET using the nonlinear Schrödinger equation obtained by perturbation. Several numerical calculations follow to validate it.

1. INTRODUCTION

Recently, soliton-like pulses in a composite right- and left-handed (CRLH) transmission line [1] have been well investigated [2–5]. Because of dispersion, a broadband pulse cannot travel on the CRLH line without distortion. The dispersion of CRLH lines can be compensated through the nonlinearity introduced by the varactors, resulting in an envelope soliton governed by the nonlinear Schrödinger equation. However, the large parasitic resistance of the inductor greatly diminishes the amplitude of the waves on the line, making the varactor's nonlinearity inefficient in compensating for the dispersion of the CRLH lines. To cancel the wave attenuation, we consider a traveling-wave field-effect transistor (TWFET) [6, 7], the gate and

Received 18 February 2011, Accepted 8 April 2011, Scheduled 12 April 2011
Corresponding author: Koichi Narahara (narahara@yz.yamagata-u.ac.jp).

drain transmission lines of which have a CRLH line structure. In this paper, we first describe the device configuration and operating principles, including the dispersion, and the properties of the one-soliton solution of the nonlinear Schrödinger equation that describes the line. We then numerically observe the cancellation of the dispersion and attenuation present in the envelope pulses.

2. FUNDAMENTAL PROPERTIES OF TWFET

Figure 1(a) shows the device structure under investigation. The parameters L_{Rg}, C_{Lg}, and L_{Lg} are the series inductance, series capacitance, and shunt inductance of the gate line, respectively. The elements subscripted with d correspond to the drain line. R_g, R_d, R_{ing}, and R_{ind} are the gate series resistance, drain series resistance, gate shunt resistance, and drain shunt resistance, respectively. The gate and drain lines are connected to the gate and drain electrodes of a FET for each cell. A FET is equivalently represented as shown in Figure 1(b). The drain-source, gate-drain, and gate-source capacitances are represented by C_{ds}, C_{gd}, and C_{gs}, respectively. The gate-source capacitance depends on the terminal voltage due to the Schottky contact interface. The drain-source current is represented by current source I_{ds}, which depends on the gate bias and drain bias voltages. Biasing voltages V_{GG} and V_{DD} can be applied to each transistor through the shunt capacitance and inductance.

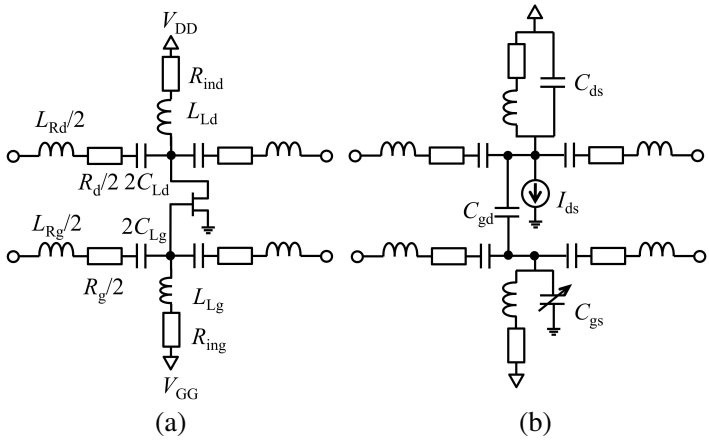

Figure 1. Unit cell of TWFET. (a) Structure and (b) equivalent representation.

Using this representation, the transmission equations are given by

$$\frac{d^2I_n}{dt^2} = -\frac{1}{L_{Rg}}\left(\frac{I_n}{C_{Lg}} + R_g\frac{dI_n}{dt} + \frac{d}{dt}(V_n - V_{n-1})\right), \quad (1)$$

$$\frac{d^2J_n}{dt^2} = -\frac{1}{L_{Rd}}\left(\frac{J_n}{C_{Ld}} + R_d\frac{dJ_n}{dt} + \frac{d}{dt}(W_n - W_{n-1})\right), \quad (2)$$

$$\begin{aligned}\frac{d^2W_n}{dt^2} &= \frac{C_{gs}+C_{gd}}{C_{gd}}\frac{d^2V_n}{dt^2} - \frac{V_{GG}-V_n}{C_{gd}L_{Lg}} \\ &\quad -\frac{1}{C_{gd}}\frac{d}{dt}(I_n - I_{n+1}) + \frac{1}{C_{gd}}\frac{dC_{gs}}{dV_n}\left(\frac{dV_n}{dt}\right)^2 \\ &\quad -\frac{R_{ing}}{C_{gd}L_{Lg}}\left(C_{gd}\frac{dW_n}{dt} - (C_{gs}+C_{gd})\frac{dV_n}{dt} + I_n - I_{n+1}\right), \quad (3)\end{aligned}$$

$$\begin{aligned}\frac{d^2V_n}{dt^2} &= \frac{C_{ds}+C_{gd}}{C_{gd}}\frac{d^2W_n}{dt^2} - \frac{V_{DD}-W_n}{C_{gd}L_{Ld}} \\ &\quad -\frac{R_{ind}}{C_{gd}L_{Ld}}\left(C_{gd}\frac{dV_n}{dt} - (C_{ds}+C_{gd})\frac{dW_n}{dt} + J_n - J_{n+1} - I_{ds}\right) \\ &\quad -\frac{1}{C_{gd}}\frac{d}{dt}(J_n - J_{n+1}) + \frac{1}{C_{gd}}\frac{\partial I_{ds}}{\partial V_n}\frac{dV_n}{dt} + \frac{1}{C_{gd}}\frac{\partial I_{ds}}{\partial W_n}\frac{dW_n}{dt}, \quad (4)\end{aligned}$$

where I_n, J_n, V_n, and W_n are the gate current at the nth cell, drain current at the nth cell, gate voltage at the nth cell, and drain voltage at the nth cell, respectively. Moreover, we define C_{gs} as

$$C_{gs}(V) = \frac{C_0}{\left(1 - \frac{V}{V_J}\right)^m}, \quad (5)$$

where C_0, V_J, and m are the zero-bias junction capacitance, junction potential, and grading coefficient, respectively. The drain-source current is defined as

$$I_{ds}(V,W) = \begin{cases} 0, & V < V_{TO}, \\ \beta(V - V_{TO})^2, & V_{TO} \le V < V_{TO} + W, \\ \beta W(2(V - V_{TO}) - W), & V \ge V_{TO} + W, \end{cases} \quad (6)$$

where V, W, β, and V_{TO} are the gate, drain voltages, transconductance coefficient, and threshold voltage, respectively. We first linearize Equations (1)–(4) to examine the dispersive property of the line. Because the line has a very complicated structure, any characterizing expressions become formidable; therefore, we hereafter confine the discussion to a TWFET with the parameters listed in Table 1 for concise illustrations. The main features are properly illustrated by the example listed in Table 1. Consistently, C_0 is set to 1.11 pF. Moreover,

Table 1. Line parameters of investigated TWFET.

L_{Rg} (nH)	2.0	L_{Rd} (nH)	1.6
C_{Lg} (pF)	0.5	C_{Ld} (pF)	1.0
L_{Lg} (nH)	1.2	L_{Ld} (nH)	0.8
$C_{gs}(V_{GG})$ (pF)	1.5	C_{ds} (pF)	1.0
C_{gd} (pF)	0.2		

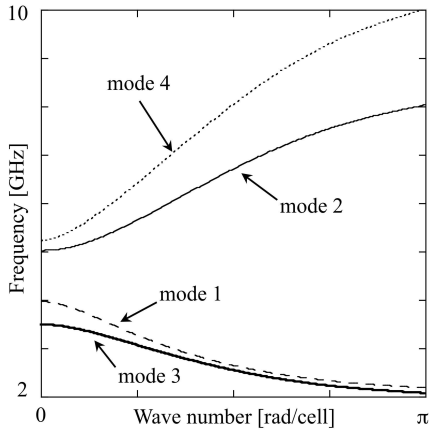

Figure 2. Typical dispersion of TWFET.

m and V_J are set to 0.5 and 2.0 V, respectively. We suppose microwave surface-mount capacitors and inductors to realize these line parameters and print-circuit-board fabrication. The dispersion relationship is then shown in Figure 2. Because of the couplings, there are at most two different modes for each frequency [8]. Note that modes 1 and 3 exhibit a left-handed property, while modes 2 and 4 exhibit right-handedness. Each mode has its own voltage fraction (= drain voltage/gate voltage) between the gate and drain lines, denoted as $R_i(\omega)$ for mode i ($i = 1$, 2, 3, 4).

In order to investigate the contributions of nonlinearity, we introduce the spatial continuous variable x, defining functions $V = V(x,t)$ and $W = W(x,t)$ as the continuous counterpart of the voltages at the nth cell V_n and W_n, respectively. Moreover, we prepare the respective spatial and temporal coordinates for the envelope and carrier waves. We use x, and t as the spatial and temporal coordinates, respectively, for the description of the carrier wave. For the envelope wave, $\xi \equiv \epsilon(x - V_g t)$, and $\tau \equiv \epsilon^2 t$ are used as the spatial and temporal

coordinates, V_g is given by $\partial_k \omega(k)$, where $\omega = \omega(k)$ denotes the dispersion relationship for wave number k. We then expand the voltage variables as

$$V = V_{GG} + \sum_{m=1}^{\infty} \epsilon^m \sum_{l=-\infty}^{\infty} v_l^{(m)}(\xi, \tau) e^{il(kx-\omega t)}, \tag{7}$$

$$W = V_{DD} + \sum_{m=1}^{\infty} \epsilon^m \sum_{l=-\infty}^{\infty} w_l^{(m)}(\xi, \tau) e^{il(kx-\omega t)}. \tag{8}$$

With these definitions, we obtain the following nonlinear Schrödinger (NS) equation with a gain term that describes $w_1^{(1)}$ by applying the reductive perturbation method [9] to Equations (1)–(4),

$$i\frac{\partial w_1^{(1)}}{\partial \tau} + p\frac{\partial^2 w_1^{(1)}}{\partial \xi^2} + q\left|w_1^{(1)}\right|^2 w_1^{(1)} + i\nu w_1^{(1)} = 0, \tag{9}$$

where p and q are the dispersion and nonlinearity coefficients. If $pq > 0$, we obtain a bright soliton solution with amplitude A given by

$$w_1^{(1)} = A\text{sech}\left(\sqrt{\frac{q}{2p}}A\xi\right)\exp\left(i\frac{qA^2\tau}{2}\right). \tag{10}$$

Therefore, when the contributions of $O(\epsilon)$ components are dominant, W is calculated as

$$\begin{aligned} W(x,t) &= V_{DD} + A_0\text{sech}\left(\sqrt{\frac{q}{8p}}A_0(x - V_g t)\right) \\ &\quad \times \cos\left\{kx - \left(\omega - \frac{qA_0^2}{8}\right)t\right\}, \end{aligned} \tag{11}$$

where $A_0 = 2\epsilon A$. Furthermore, we observe that each mode can support a soliton-like pulse, and the soliton-like pulse carried by mode i ($i = 1$, 2, 3, 4) has the voltage fraction of R_i between the gate and drain lines.

For the line parameters listed in Table 1, the properties of a one-soliton solution are shown in Figure 3. The pulse width and voltage fraction between the lines are shown by the solid and dashed curves. The one-soliton solutions carried by modes 1, 2, 3, and 4 are shown in Figures 3(a), (b), (c), and (d), respectively. In the shaded regions, the product pq becomes negative; therefore, the bright solitons cannot develop.

The attenuation factor ν of the one-soliton solutions carried by modes 1, 2, 3, and 4 are shown in Figures 4(a), (b), (c), and (d), respectively. The wave losses are mainly caused by the parasitic resistances of inductors. Generally, the resistances tend to be proportional to the corresponding inductances. We thus set R_g,

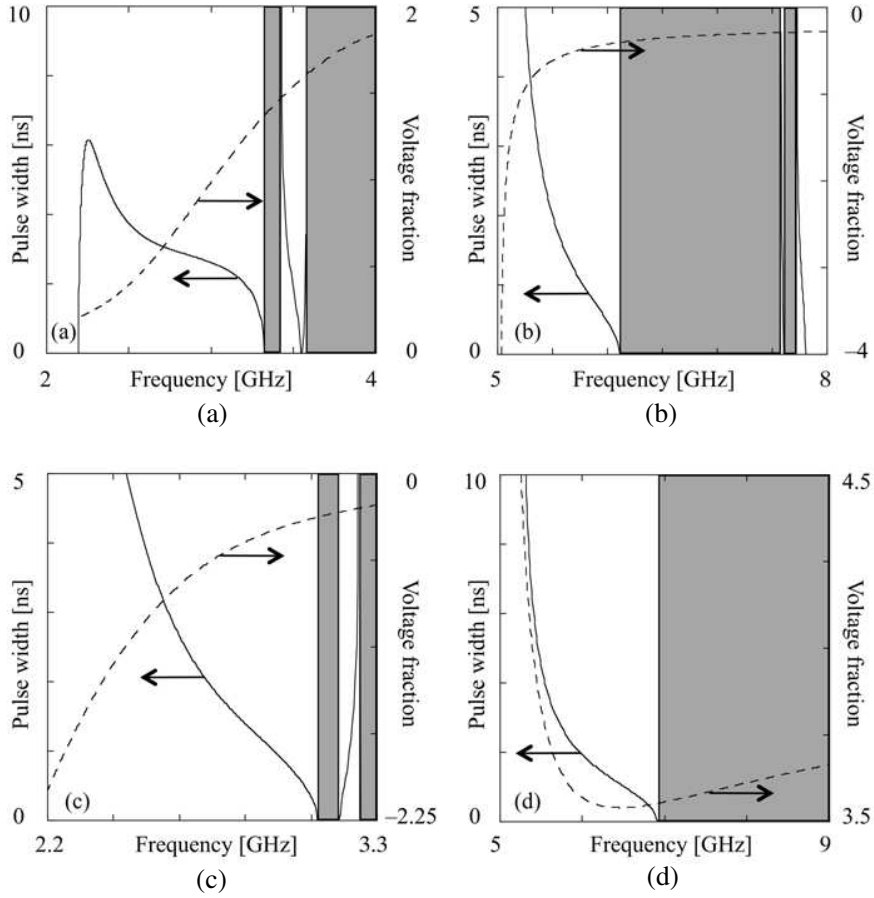

Figure 3. Properties of bright one-soliton solution.

R_d, R_{ing}, and R_{ind} to 0.04, 0.032, 0.024, and 0.016 Ω, respectively. Moreover, V_{TO}, V_{GG}, and β to −1.0 V, −0.9 V, and 1.0 mAV^{-2}, respectively. Note that the pulse becomes amplified when $\nu < 0$. For the present parameters, amplified pulses can be observed only in a bounded frequency range of mode 3.

3. NUMERICAL EVALUATION

We numerically solve Equations (1)–(4) using the standard finite difference method [10] to determine the capability of the line to support unattenuated dispersion-free envelope pulses, and examine the validity

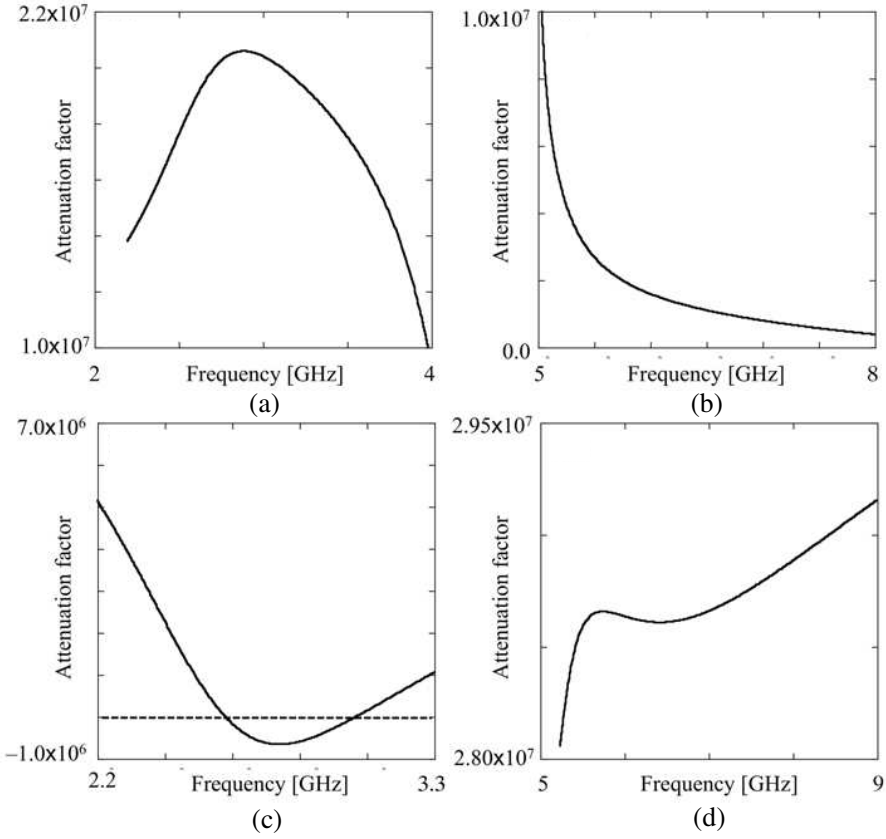

Figure 4. Amplification of nonlinear pulse by FET contributions.

of the design criteria discussed above. We discuss the results for the parameters in Table 1.

Figure 5 compares the pulse traveling in the linear and nonlinear TWFETs. The losses and drain-source current were all set to zero. The carrier frequency was set to 2.8 GHz and the input voltage fraction between the gate and drain lines was set to R_3 ($= -0.5$), such that the pulse is supposed to be carried by mode 3. Moreover, for the linear line, the gate-source capacitance was fixed at $C_{gs}(V_{GG})$. Five temporal waveforms recorded at $n = 200$, 600, 1000, 1400 and 1800 are shown for the drain line. We can see that the pulse spreads due to dispersion in Figure 5(a). The dispersive distortion is successfully cancelled by the nonlinearity in Figure 5(b). The nonlinear pulses monitored at $n = 1800$ are shown in Figure 6 with

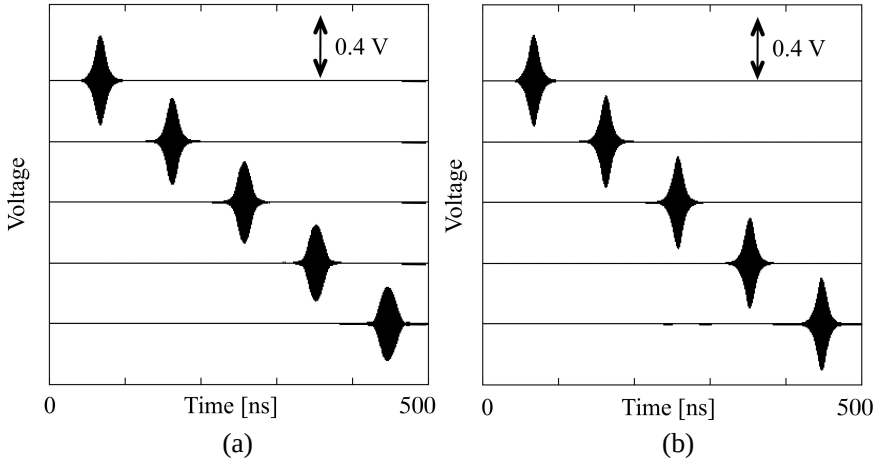

Figure 5. Compensated dispersion of nonlinear pulse. Numerically obtained waveforms for (a) linear and (b) nonlinear lines.

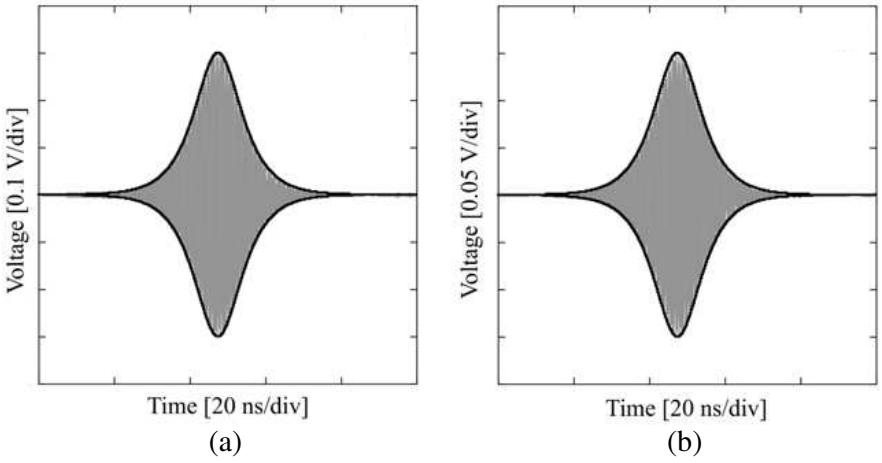

Figure 6. Comparison between analytical and numerical pulses.

analytical envelope waveforms given by Equation (11). Figures 6(a) and (b) are the waveforms on the gate and drain lines, respectively. The numerical waveforms are represented by gray curves. Only the envelopes are shown for the analytical waveforms by the solid curves. Originally, Equation (11) describes a soliton-like pulse having a small amplitude that can be treated perturbatively. However, the numerical waveforms are well characterized by the analytical ones. Although

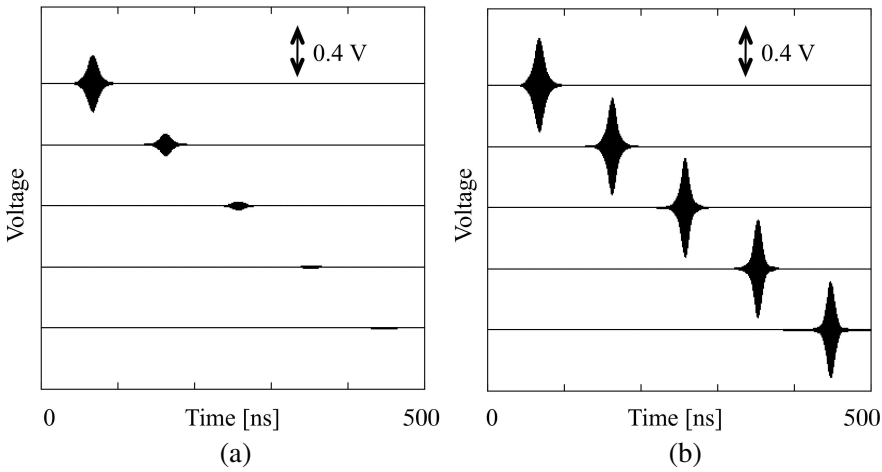

Figure 7. Numerical observation of loss-compensated nonlinear pulse. Loss line (a) without (b) with FET gain.

not explicitly described, the similarity between the numerical and analytical waveforms has been well established for several sets of line parameters other than those in Table 1. On the other hand, because of the asymmetric capacitance-voltage relationship of the Schottky varactors, some numerical waveform observed in the gate line is also asymmetrical in amplitude.

Finally, we discuss the loss-compensation in TWFETs. We set R_g, R_d, R_{ing}, and R_{ind} to 0.04, 0.032, 0.024, and 0.016 Ω, respectively. Figure 7 shows the contribution of FET gain to dispersion-free pulse propagation. Five waveforms on the drain line recorded at $n = 200$, 600, 1000, 1400 and 1800 are shown. Figure 7(a) corresponds to the case where β is set to zero. The pulse is simply attenuated to disappear at $n = 1000$. On the other hand, we set $\beta = 0.79\,\mathrm{mAV}^{-2}$ in Figure 7(b) such that the attenuation factor ν becomes almost zero. We can see that the unattenuated shape-invariant pulse travels in TWFETs. This observation verifies the potential of TWFETs to support unattenuated dispersion-free envelope pulses.

4. CONCLUSION

We characterized TWFETs, each electrode line of which has the same unit-cell structure as a CRLH line, to develop unattenuated dispersion-free pulses. Using design parameters such as the dispersion coefficient p, nonlinearity coefficient q, and attenuation factor ν, we

can freely design the length or area of a platform for dispersion-free pulse propagation. We believe that this may significantly increase the applications of nonlinear pulses in high-speed electronics.

REFERENCES

1. Caloz, C. and T. Itoh, *Electromagnetic Metamaterials: Transmission Line Theory and Microwave Applications*, Wiley-Interscience, New York, 2006.
2. Gupta, S. and C. Caloz, "Dark and bright solitons in left-handed nonlinear transmission line metamaterials," *Proc. IEEE MTT-S Int'l. Microwave Symp. 2007*, 979–982, Honolulu, 2007.
3. Kafaratzis, A. and Z. Hu, "Envelope solitons in nonlinear left-handed transmission lines," *Proc. Metamaterials 2007*, 771–773, Rome, Oct. 22–24, 2007.
4. Gharakhili, F. G., M. Shahabadi, and M. Hakkak, "Bright and dark soliton generation in a left-handed nonlinear transmission line with series nonlinear capacitors," *Progress In Electromagnetics Research*, Vol. 96, 237–249, 2009.
5. Ogasawara, J. and K. Narahara, "Short envelope pulse propagation in composite right- and left-handed transmission lines with regularly spaced Schottky varactors," *IEICE Electron. Express*, Vol. 6, 1576–1581, 2009.
6. McIver, G. W., "A traveling-wave transistor," *Proc. IEEE*, Vol. 53, 1747–1748, 1965.
7. Narahara, K. and S. Nakagawa, "Nonlinear traveling-wave field effect transistors for amplification of short electrical pulses," *IEICE Electron. Express*, Vol. 7, 1188–1194, 2010.
8. Gupta, K. C., R. Garg, and I. J. Bahl, *Microstrip Lines and Slotlines*, Artech, 1979.
9. Taniuti, T., "Reductive perturbation method and far fields of wave equations," *Prog. Theor. Phys. Suppl.*, Vol. 55, 1–55, 1974.
10. Paul, C. R., *Analysis of Multiconductor Transmission Lines*, Wiley-Interscience, New York, 1994.